de Haas–van Alphen scattering measurements on the reentrant superconductor $La_{1-x}Ce_xAl_2$

S. I. Epstein, R. J. Higgins, and D. H. Lowndes*
Department of Physics, University of Oregon, Eugene, Oregon 97403-1274

F. Steglich
Institut für Festkörperphysik, Technische Hochschule Darmstadt, D-6100 Darmstadt, West Germany

J. F. Smith
Ames Laboratory, Iowa State University, Ames, Iowa 50011
(Received 11 March 1985; revised manuscript received 3 September 1985)

de Haas–van Alphen quantum oscillations have been seen for the first time in single crystals of $LaAl_2$ heavily doped with the magnetic impurities Ce and Gd. Spin-split zeros have been detected on the Γ-centered sheet of the Fermi surface in pure $LaAl_2$. These change to spin-split minima in the doped crystals. From these observations, along with orbitally averaged effective-mass measurements, estimates have been made of the g-value shift and the spin-dependent scattering due to the presence of the rare-earth impurities. Measurements of the scattering rate were made, as a function of temperature, in the 0.5 at. % Ce and the 0.5 at. % Gd impurity-doped crystals, for two orbits. An orbit selected for high s-p–wave character showed no temperature dependence for either impurity, whereas an orbit selected for high d-f character showed Kondo-like behavior for both the Ce- and the Gd-doped crystals. This is in contrast to the resistivity, which has a Kondo-like behavior for Ce but not for Gd doping. Dingle-temperature anisotropy has been studied on the Γ-centered sheet of the Fermi surface for the 0.3 at. % Ce and the 0.5 at. % Gd impurity-doped crystals, with use of three orbits of qualitatively different symmetry character. Data from the Ce-doped sample indicate the presence of extreme spin-dependent scattering for the orbit passing through four ⟨100⟩ directions in **k** space, which include a strong f-wave component. This behavior is consistent with the spin-split-minimum rotation diagrams, which show increased spin-dependent scattering as one proceeds in the direction of increasing f-wave character from ⟨111⟩ to ⟨100⟩ in the (110) plane.

I. INTRODUCTION

The superconductor $LaAl_2$, when doped with small amounts of Ce (0.6–0.7 at. % substitution for La) is found to exhibit the characteristics of reentrant superconductivity. A reentrant superconductor has the following properties: The material has an initial superconducting transition temperature, T_{c1}; if the sample is further cooled, it returns to its normal state at temperature T_{c2}; if cooled still further, it once again becomes superconducting at temperature T_{c3} (the existence of T_{c3} has not yet been detected in $LaAl_2$). Such behavior was theoretically predicted by Mueller-Hartmann and Zittartz[1] (MH-Z) to occur in magnetically-doped superconducting materials which, in their normal state, exhibit the Kondo effect, provided that $T_K \ll T_{c1}$. Here T_K is the Kondo temperature, $T_K \propto T_F \exp[-1/|J_{s-f}|N(E_F)]$, where T_F is the Fermi temperature, J_{s-f} is the coupling strength parameter for the interaction between conduction electrons and the f-electron local moment, and $N(E_F)$ is the density of states at the Fermi energy, E_F.

The MH-Z theory is based on the assumption of a spherical Fermi surface for the host matrix. Results of recent theoretical calculations,[2,3] as well as experimental Fermi surface mapping of $LaAl_2$ (Refs. 4 and 5) indicate an extremely complex Fermi surface (Fig. 1). In an effort to better understand the mechanisms involved in reentrant superconductivity, a study was undertaken to measure electron scattering anisotropy over the anisotropic Fermi surface of $LaAl_2$ doped with Ce and Gd.

The technique employed in this study was the de Haas–van Alphen (dHvA) effect. Although originally used primarily to map out Fermi surface dimensions in metals, the dHvA effect is an effective tool for measuring electron scattering lifetimes due to the presence of impurities.[6] The most general expression for dHvA oscillations in a metal, in the presence of magnetic impurities, is

$$\mathbf{M} = -(\hat{\mathbf{m}}/2)\sum_{\sigma}\sum_{r=1}^{\infty} C_r D^r E^{\sigma r} \sin[2\pi r(F/H-\gamma) + p\pi/4 - \sigma\pi r S'] , \quad (1)$$

where **M** is the magnetization, r is the dHvA harmonic index, F is the dHvA frequency ($=\hbar cA/2\pi e$), A is the extremal cross-sectional area of the Fermi surface normal to the magnetic field, H is the magnetic field, γ is the Onsager phase factor ($=\frac{1}{2}$ for free electrons), $p=-1(+1)$ for maximal (minimal) cross-sectional areas, C_r is the dHvA amplitude reduction factor due to finite temperature,

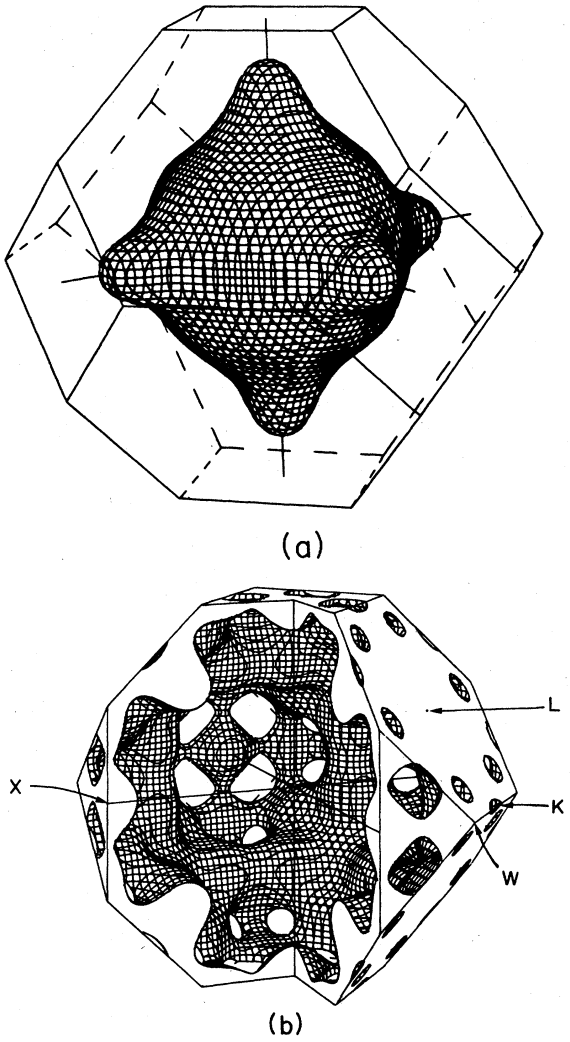

FIG. 1. (a) Perspective of the tenth-band electron sheet of the Fermi surface for $LaAl_2$ (from Ref. 2). (b) Perspective of the ninth-band multiply connected hole sheet of the Fermi surface for $LaAl_2$ (from Ref. 2).

$$C_r=\nu(TF)/(A''rH)^{1/2}[1/\sinh(rK_0m^*T/H)] ,$$

$$\nu=[4k_B/(2\pi)^{1/2}](e/\hbar c)^{3/2}$$

$$=1.30\times10^{-5}\ \mathrm{Oe}^{1/2}/\mathrm{K} ,$$

$$K_0=2\pi^2k_Bm_0c/e\hbar=146.9\ \mathrm{kOe/K} ,$$

$$A''=|d^2A/dk_H{}^2| ,$$

$$\hat{\mathbf{m}}=\hat{\mathbf{H}}-(1/F)(\partial F/\partial\theta)\hat{\boldsymbol{\theta}}-(1/F\sin\theta)(\partial F/\partial\phi)\hat{\boldsymbol{\phi}} ,$$

$\sigma=-1\ (+1)$ for spin-down (-up) electrons ,

$$D=\exp(-rK_0m^*X_{\mathrm{avg}}/H) ,$$

$$E=\exp(-K_0m^*\delta x/H) ,$$

$$S'=(m^*/2)(g+H_{\mathrm{ex}}/H) .$$

The quantity m^* is the orbitally-averaged effective mass of an electron for the extremal orbit in question (in units of m_0), m_0 is the mass of the electron, c is the speed of light, g is the electronic cyclotron orbitally-averaged g factor, and k_B is Boltzmann's constant. X_{av} is the average Dingle temperature for spin-up ($\uparrow$) and spin-down ($\downarrow$) electrons: $X_{\mathrm{av}}=(X_{d\uparrow}+X_{d\downarrow})/2$, where X_d, the Dingle temperature, is defined as

$$X_d=(\hbar/2\pi k_B)[1/\tau(\mathbf{k})] ,$$

and $\tau(\mathbf{k})$ is the electronic scattering lifetime at a point $\mathbf{k}$ on the Fermi surface. The quantity $2\delta x=X_{d\uparrow}-X_{d\downarrow}$ is the difference in X_d of the two scattered components. $H_{\mathrm{ex}}=E_{\mathrm{ex}}/u_B$, where E_{ex} is the exchange energy between the impurity and the conduction electrons, and u_B is the Bohr magneton.[7]

The Fermi surface of $LaAl_2$, depicted in Fig. 1, consists of (1) a closed, Γ-centered electronlike sheet, arising from the tenth band, which is nearly circular in shape, with bumps in the $\langle 100\rangle$ directions; (2) a multiply-connected holelike sheet, formed from the ninth band; and (3) a set of hole pockets (not shown in Fig. 1) surrounding the points labeled L. Comparison of theoretically derived extremal areas[2] with experimentally measured extremal areas[4] shows good qualitative agreement (see Fig. 2).

Maple and Smith[8] suggested that interaction of $LaAl_2$ with Ce impurities proceeds mainly via conduction electrons having a high degree of f-partial-wave character. They proposed that the interaction occurs via covalent mixing of impurity energy levels with f-wave conduction-electron levels. In support of this argument they made measurements[8] indicating a pressure dependence of T_{c1} for $La_{1-x}Ce_xAl_2$. No pressure dependence of T_{c1} is found for $La_{1-x}Gd_xAl_2$, a superconductor which is not of the reentrant type, but which instead exhibits a depression of T_c versus impurity concentration typical of ferromagnetic impurities (as predicted by Abrikosov and Gor'kov[9]). According to Maple and Smith, the pressure dependence of the Ce alloy is associated with a relative energy-level shift between f-character impurity energy levels and host conduction-electron energy levels of large f-wave character, which alters the overlap, and resonant interaction. Seitz *et al.*[4] have suggested that electrons with large f-wave character can be found at the $\langle 100\rangle$ bumps of the Γ-centered electron sheet, and also on the smaller, holelike pieces of Fermi surface.[10]

The dHvA effect provides a microscopic probe of the interaction between impurities and host matrix conduction electrons of varying symmetry character, since (a) the frequency spectrum allows orbits of different symmetry character to be studied separately, and (b) for each orbit the g factor, scattering rate, and spin dependence of scattering may be determined.[6]

The subset of orbits chosen for study was limited to those orbits which could give adequate spectral resolution for accurate measurements of dHvA signal amplitude. The following dHvA orbits were chosen for observation of electron scattering. The normal to each planar orbit lies in the (110) plane in $\mathbf{k}$ space.

(a) One orbit is the extremal orbit on the Γ-centered sheet whose normal is the [100] direction in $\mathbf{k}$ space; this

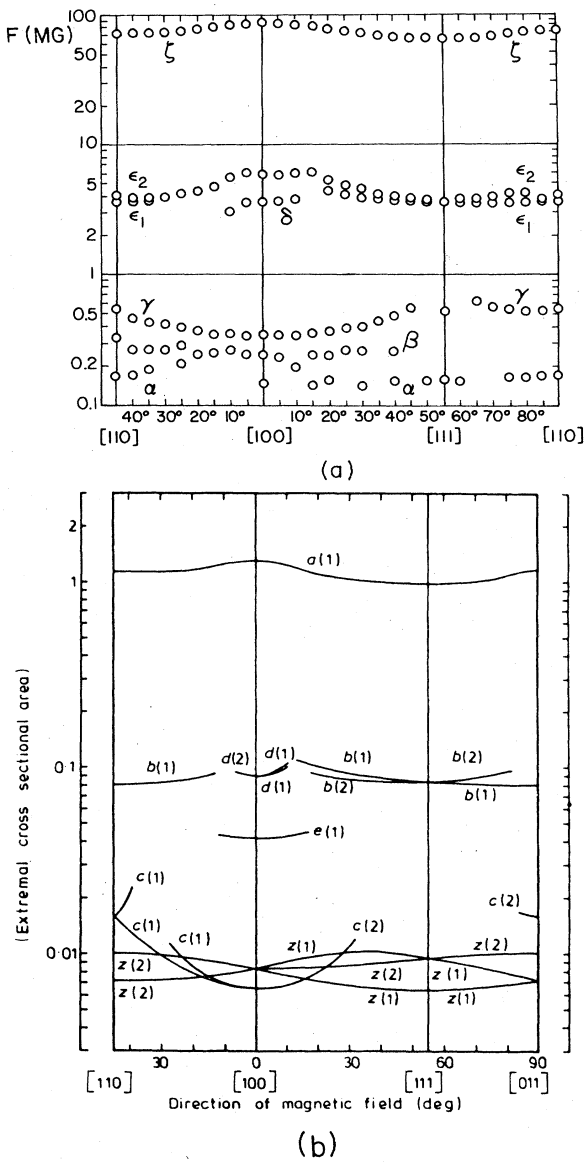

FIG. 2. (a) dHvA measured frequencies of $LaAl_2$ for orbits in the (110) and (100) planes (from Ref. 4). (b) Theoretically derived extremal areas for $LaAl_2$ (from Ref. 2).

orbit passes through four ⟨100⟩ directions.

(b) A second orbit is the orbit on the Γ-centered sheet, whose normal is the [111] direction in **k** space; this orbit passes through no ⟨100⟩ directions.

Orbits (a) and (b) were chosen for observation because it was expected that scattering of electrons due to Ce for orbit (a), which contains four f-like "bumps," would be greater than scattering for orbit (b), which is circular (free-electron-like).[4]

(c) A third orbit is the orbit on the Γ-centered sheet, whose normal is at an angle of 15° to the [100] direction. This orbit was selected for observation because preliminary theoretical calculations[11] indicate that d-wave character increases as one proceeds from the direction [111] to [100] in the (110) plane, whereas f-wave character is sharply peaked within 15° of [100]. In order to distinguish d-wave scattering from f-wave scattering, orbit (c), which does not pass through the ⟨100⟩ f-like bumps, was chosen for comparison to orbits (a) and (b).

(d) A fourth orbit is the orbit on the smaller, holelike piece of Fermi surface, whose normal is the [100] direction in **k** space, and whose dHvA frequency is 0.35 mG. We expected that scattering of electrons on this orbit would be greater than that of orbit (b), due to the expected higher f-wave character of the smaller pieces of Fermi surface, as compared with the free-electron-like orbit (b).[3,4]

It is to be noted here that we are not aware of any augmented-plane-wave (APW) partial-wave analysis calculations for dHvA orbits on the Fermi surface of $LaAl_2$. In the absence of such calculations, it was felt that the orbits (a) and (d) chosen for study would show the greatest scattering effects due to the interaction of Ce with those electrons having large f-wave character.

In addition to studying Ce-doped $LaAl_2$, one sample of Gd-doped $LaAl_2$ was chosen for study to contrast the behavior of the antiferromagnetic (AF) dopant Ce on the host matrix $LaAl_2$. As was mentioned above, gadolinium behaves as a ferromagnetic (F) dopant in $LaAl_2$;[12] it does not produce the reentrant superconductive phenomenon.

As no dHvA experiments had been done on $La_{1-x}R_xAl_2$ (R=Ce,Gd) crystals prior to this work, selection of the range of impurity concentrations for study was a nontrivial problem. Dilute alloy samples were required which would (1) exhibit rare-earth (RE) interactions with conduction electrons, (2) be in the single ion (no impurity-impurity interaction) region, and (3) not be so high in RE concentration as to obliterate dHvA signals. Past work on these compounds[13,14] indicated that, for concentrations $x \leq 0.5$ at.%, Ce and Gd (substituting for La) behave as single-impurity scatterers. The other requirements, (1) and (3) above, were also fortuitously satisfied by the crystals which were chosen for this study.

Single crystals of $LaAl_2$ and $La_{1-x}R_xAl_2$ (R=Ce,Gd) were prepared using the Czochralski technique.[15] They were then annealed under a vacuum of $\sim 2\times10^{-6}$ Torr, in order to improve the residual resistance ratio $\mathscr{R}$. During annealing, each sample was wrapped successively with Ta, Zr, and Ta foils (based on annealing techniques described in Refs. 16 and 17). The final sample dimensions were approximately $1\times1\times3$mm.

The set of samples chosen for this work was the following:

(1) $LaAl_2$, annealed 48 h, 1000°C $\mathscr{R}=655$; long axis equal to ⟨110⟩.

(2) $La_{0.997}Ce_{0.003}Al_2$, annealed 72 h, 900°C $\mathscr{R}=155$; long axis equal to ⟨111⟩.

(3) $La_{0.995}Ce_{0.005}Al_2$, annealed 24 h, 700°C $\mathscr{R}=79.5$; long axis equal to ⟨110⟩.

(4) $La_{0.995}Gd_{0.005}Al_2$, annealed 96 h, 900°C $\mathscr{R}=65$; long axis equal to ⟨111⟩.

II. OBSERVATIONS

Three types of measurements were made: (i) detection of spin-split zeros, and of their angular shifts with vary-

ing alloy composition; (ii) measurement of scattering lifetime versus temperature for various orbits; and (iii) measurement of X_d anisotropy.

A. Spin-split zeros

After it was determined that oscillations could be seen in the pure crystal, a search for spin-split zeros (SSZ's) on the Γ-centered sheet was carried out. A spin-split zero is a null in dHvA signal amplitude which occurs when the contributions from spin-up and spin-down electrons completely cancel. If one knows the effective mass for the orbit in question, the possible values for the orbitally-averaged g factor can be obtained from the expression $g_0 m^* = N$, where $N = 1,3,5,7,\ldots$.[18]

A SSZ can be used as a reference point from which to measure the exchange energy due to the presence of the magnetic impurity. In the case where a magnetic impurity is present, the SSZ condition becomes

$$g' m^* = N \ , \tag{3}$$

where $g' = g_0 - (E_{ex}/u_B H)$ for antiferromagnetic exchange, and $g' = g_0 + (E_{ex}/u_B H)$ for ferromagnetic exchange. In the event that the spin-up and spin-down electrons are not scattered equally, there is an incomplete cancellation of the resultant dHvA signal; the resulting feature is called a spin-split minimum (SSM).[18]

The search for a spin-split zero was prompted by the knowledge[4] that $m^* = 1.52$ in the [111] direction for the Γ-centered sheet. This value of m^*, combined with the free-electron g factor $g \cong 2.0$, suggests the likely occurence of an SSZ at some point on this sheet of the Fermi surface, since the product $g_0 m^*$ would be expected to be nearly 3 at [111].

The search did in fact lead to the discovery of a spin-split zero; a second zero also appeared in this search, as can be seen in Fig. 3(a). A similar search for the shifted SSZ's in the impurity crystals produced the rotation diagrams shown in Figs. 3(b), 3(c), and 3(d). The possibility that the existence of the SSZ's was in fact spurious, and resulted from mosaic or bicrystalline substructure within the samples measured, was rejected because (a) minima were seen in all four of the crystals studied, and (b) in the two Ce-doped crystals studied, two successive minima were observed at angles which were only slightly shifted from those of the SSZ's in the pure crystals. Both mosaic and bicrystalline substructure, in general, cause the random appearance of amplitude minima within a dHvA rotation diagram,[19] contrary to the consistent appearance of SSM's in all samples measured in this work. Results are summarized in Table I.

A technique developed by Coleridge, Scott, and Templeton[18] allows one to measure spin-dependent scattering from observation of signal amplitude at a spin-split minimum and at nearby angles. The measurements are limited to angles near the minimum, where the amplitude can be obtained as the difference of two interfering sine waves. A measurement at the minimum determines the difference in the amplitudes; a second amplitude measurement a few degrees away gives the second piece of information sufficient to determine the ratio of the amplitudes,

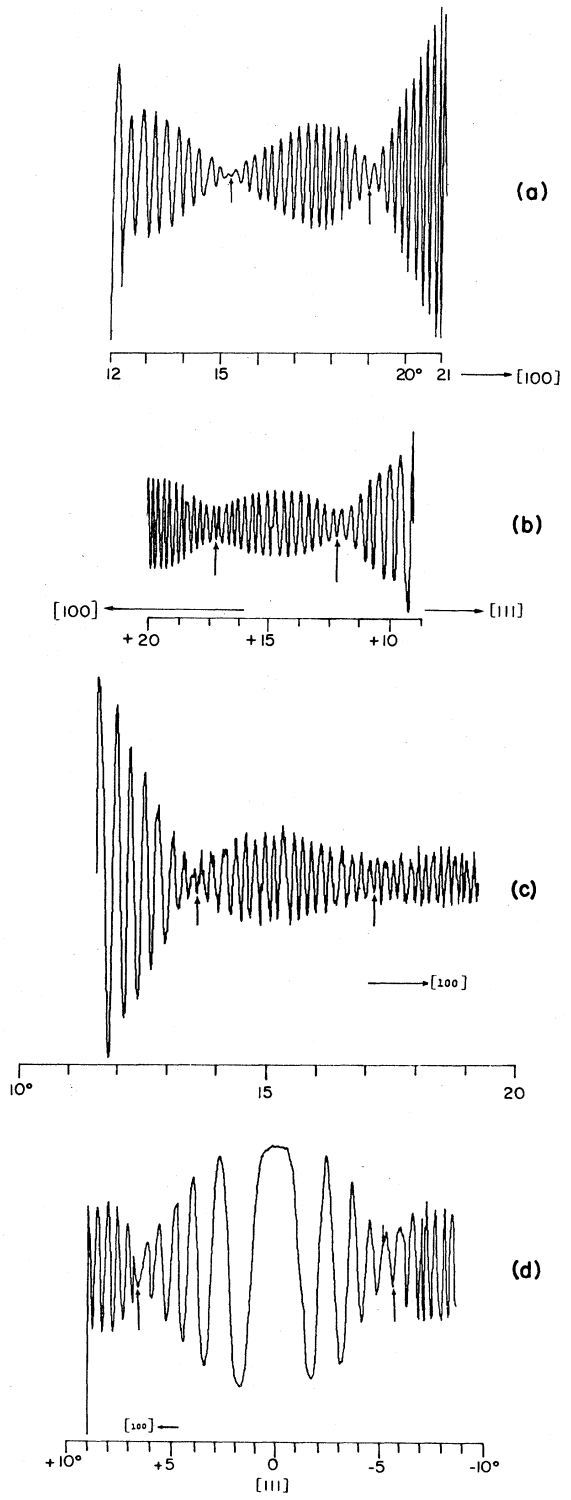

FIG. 3. Rotation diagrams showing SSZ's in $LaAl_2$, and corresponding SSM's in the alloy crystals. Position of each SSZ (SSM) is indicated by an arrow. Origin of each graph is [111]. All angles are measured in units of degrees. (a) Pure $LaAl_2$, two SSZ's. (b) 0.3 at. % Ce alloy, two SSM's. (c) 0.5 at. % Ce alloy, two SSM's. (d) 0.5 at. % Gd alloy, one SSM on each side of the [111] symmetry direction. (Scales differ for each of the graphs.)

TABLE I. SSZ's and SSM's observed in $LaAl_2$, $LaCeAl_2$, and $LaGdAl_2$.

Angle (deg)	Magnetic field (kG)	δx (K)	Temp. (K)	m^*/m_0	g'	g_0	$\Delta g \equiv g'-g_0$	$H_{ex} \equiv H(\Delta g)$ (kG)	$\delta H_{ex} \equiv H(\delta \Delta g)$ (kG)
				First SSM (Assuming $m^*g_0=3$)					
				Pure					
+15.2	72.1	SSZ	1.25	1.59		1.89			
				0.3 at. % Ce					
+13.3	84.4	0.038	0.54	1.56	1.92	1.62	+0.30	25.3	16.0
+11.5	74.9	0.022	1.18	1.54	1.95	1.37	+0.58	43.4	14.2
				0.5 at. % Ce					
+12.4	84.4	0.0099	0.54	1.55	1.94	1.50	+0.44	37.1	16.0
+12.7	84.4	0.017	1.15	1.55+	1.94−	1.54	+0.40	33.8	16.0
				0.5 at. % Gd					
−5.5	84.4	0.001 77	0.54	1.53	1.96				
+5.6	84.4	0.001 77	0.54	1.53	1.96				
+7.5	84.4	0.0050	1.28	1.53+	1.96−				
−6.4	84.4	0.0013	1.28	1.53	1.96				
−4.5	56.3	0.001 77	0.54	1.53	1.96				
−31.0	84.4	a	0.54	~2.14	1.36				
				Second SSM (Assuming $m^*g_0=5$)					
				Pure					
+19.2	72.1	SSZ	1.25	2.04		2.45			
				0.3 at. % Ce					
+18.5	84.4	0.42	0.54	2.01	2.50	2.35	−0.15	12.7	18.6
+19.0	74.9	0.31	1.18	2.03	2.46	2.42	−0.04	2.99	16.5
				0.5 at. % Ce					
+18.0	84.4	0.39	0.54	2.02	2.47	2.28	−0.19	16.0	18.6

[a]No m^* versus θ data available near this orbit.

which in turn is directly related to δx, the amount of spin-dependent scattering, as follows:

$$\delta x = (H/K_0 m^*)2/\{-1+[1+(4c/R^2)]^{1/2}\}\ , \qquad (4)$$

where H is the value of the magnetic field, R is the magnitude of the signal at the minimum, and $c=(R'^2-R^2)/(\Phi)^2$, R' is the amplitude of the signal at a point near the minimum, and Φ is the phase of the signal measured from the minimum: $\Phi=\pi(m^*g'-1)$.

In practice, in order to evaluate δx, a knowledge of the variation of orbital effective mass, m^*, with rotation angle is necessary. As this information has not been measured previous to this work, effective-mass measurements were made at four points at intervals of 5°, beginning with [111]+5°. [In addition, effective masses were measured for several other points on the Γ-centered sheet; these were needed in order to evaluate X_d, for use in measurements of X_d anisotropy (Sec. II C).] All effective masses were measured by varying sample temperature between 2.0 and 1.1 K. The measured values appear in Fig. 4. Also plotted in Fig. 4 are the theoretically calculated values of m^*,[20] scaled to the measured value at [111], so as to include the effect of the electron-phonon interaction. This scaling is necessary in order to compare these "bare mass" numbers with dHvA measured values. (For a discussion of electron-phonon interaction in the dHvA effect, see Refs. 6 and 21.) The effective masses at angles lying between the measured values were obtained by linear interpolation of the measured values.

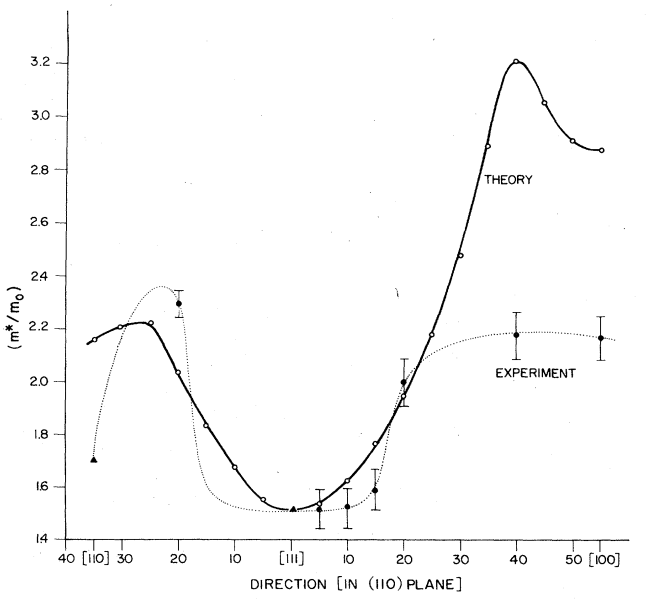

FIG. 4. Experimentally determined orbital effective masses on the Γ-centered sheet. (Values at [111] and [100] taken from Ref. 4.) Also plotted are theoretically calculated values of orbital effective mass (from Ref. 20). Angles are measured in units of degrees.

The values of δx were calculated at the SSM's for several values of R' at angles close to the SSM, using the interpolated values of effective mass; the results were then averaged. Due to the difficulty in estimating amplitude of the dHvA signal at a given point on the rotation diagrams, values of δx are at best an indication of the order of magnitude of the spin-dependent scattering. The values of g' were calculated assuming the relation $m^*g'=3$ for the first SSM, and $m^*g'=5$ for the second SSM. The values of g_0, the g factor in pure $LaAl_2$, were calculated by assuming a linear variation of g_0 between angles at which the first and second SSZ's (where $m^*g=3$ and $m^*g=5$, respectively, see discussion below) were seen in the pure crystal. The values of $H_{ex}=E_{ex}/u_B$, where E_{ex} is the exchange energy of the impurity-conduction-electron interaction, were calculated from $g'=g_0-(E_{ex}/u_BH)$.

δH_{ex}, the error associated with H_{ex}, was calculated using estimates of error in the values of g' and g_0 introduced from errors in m^* interpolation, as follows: A value of g' for one of the SSM's in the Ce-doped alloy was arrived at using relation (3) and a value of m^* interpolated from the measured effective masses. An error of dm^* in the interpolated effective mass results in $dg'=-(g'/m^*)dm^*$. In a similar fashion, using data taken on the undoped sample, $dg_0=-(g_0/m^*)dm$. $\delta H_{ex}=H(\delta\Delta g)=H(dg'-dg_0)$ is then determined.

In order to conclude from rotation diagram data that a shift in the angular position of a SSZ implies F or AF exchange, one must know g_0, the value of the g factor for the pure material, for the same orbit at which the *shifted* SSZ (or SSM) occurs. In the case of some metals, notably copper, it is known by independent measurement[22] that the g factor of the pure metal is practically constant for orbits in the region of a SSZ. Consequently a shift in the angular position of the SSZ due to the presence of a magnetic impurity, such as in the alloy Cu-Cr, can be unambiguously interpreted as an antiferromagnetic shift.[18] For the case of $LaAl_2$, no values of orbitally-averaged g factor have been previously measured. The presence of two SSZ's within 5° of one another, in a region where m^* is rapidly varying, necessarily implies that g_0 is varying rapidly with θ, where θ is the angle of rotation in the magnetic field; this rapid variation is necessary in order that relation (3) be satisfied for two different values of N. Assuming a linear variation of $g(\theta)$ between the two SSZ's, the ambiguity in the value of the g factor as obtained from the relation $m^*g=1,3,5,\ldots$, introduces ambiguity in the slope of the $g(\theta)$ curve. Hence the sign of the magnetic impurity-conduction-electron exchange, H_{ex}, cannot be determined uniquely from the rotation diagrams alone, because for one choice of end points of the $g(\theta)$ curve $g'-g_0>0$, whereas another choice of end points will result in $g'-g_0<0$. However, plausible inferences can be made which point the way for future study.

It will be assumed in this analysis that the first SSZ corresponds to $g_0m^*=3$, while the second SSZ corresponds to $g_0m^*=5$. In this way the g_0 value for each of these orbits is close to the free-electron value $g_0=2.0$. g values may differ from 2.0 from simple interband terms in the band structure near a degeneracy (absent here), or due to electron-electron interactions.[6] While we are unaware of a direct calculation of exchange-enhanced g_0 values in $LaAl_2$, and crystal purity does not permit g_0 measurement by conduction-electron spin resonance (CESR), the change in orbit character when going from [111] (s-p-like) towards [100] (d-f-like) suggests that exchange enhancement will pull g_0 upwards, not downwards. If this supposition is correct, then accepting the upper g_0 value of ~ 2.4 for the second SSZ gives a plausible basis for interpolation of g_0 at other angles in the Ce alloys.

With this assumption, along with the assumption of a linear variation of $g(\theta)$ at angles near the SSZ's of the pure $LaAl_2$, we can see, from Table I, the following.

1. Ce alloys

The g shift for both the 0.3 at. % Ce and the 0.5 at. % Ce alloys is *positive* for the first SSM. This implies a *ferromagnetic* interaction between Ce and the host conduction electrons. The g shift for the Ce alloys at the second SSM is, within error limits, approximately zero.

A possible explanation which is consistent with the above results is as follows: It is well known[23–25] that the exchange coupling strength parameter, J_{ex}, can be expressed as follows:

$$J_{ex}=J_{ferro}+J_{covalent}\ , \tag{5}$$

where J_{ferro}, the positive part of the exchange constant, is mediated between host conduction electrons and magnetic impurities through the s and d partial waves, whereas $J_{covalent}$ is mediated through the p and f partial waves.[26,27] The d-wave character on the Γ-centered sheet in the region of [111] is much larger than is the f-wave character: preliminary theoretical estimates[11] are $\langle l=3\,|\,\psi\rangle=0.03$, $\langle l=2\,|\,\psi\rangle=0.21$. Hence, even a relatively large $J_{covalent}$ has little effect on the g factor shift when compared with the contribution of J_{ferro}, due to the greater amount of d character in the wave function.

The fact that X_d versus T measurements (Sec. II B, below) indicate no Kondo-like behavior in the 0.5 at. % Ce alloy at [111] on the Γ-centered sheet lends support to the positive g shift obtained by this analysis. g-factor measurements in the pure crystal, which can be obtained by harmonic ratio measurements[6] (at lower temperatures and higher magnetic fields than are possible with the present experimental apparatus) would resolve the question of g shift.

The difference between X_d for spin-up and spin-down electrons, δx, in the Ce alloys is in all cases small and *increases* as one proceeds in the direction from [111] towards [100] in the (110) plane.

2. Gd alloy

The first SSM is located at an angle very close to [111], where the variation of m^* with angle is very small. Hence the value for δx calculated from Eq. (4) [under the assumption that $g(\theta)\sim$const in this region] is $\delta x\cong 0$.

B. Scattering lifetime versus temperature

The dHvA measurable quantity known as the Dingle temperature, X_d, is inversely proportional to the lifetime

$\tau(\mathbf{k})$, of an electron in its "racetrack" orbit, as seen in Eq. (2). It can be thought of as representing the $\mathbf{k}$-dependent resistivity for electrons in the host. Maple's[14] measurements of bulk resistivity versus temperature indicated the presence of a pronounced Kondo minimum for Ce-doped $LaAl_2$ alloys. It is reasonable to assume that this same resistivity minimum should be visible, on a microscopic basis, for those electrons which participate in the Kondo effect, and should be absent for those electrons which do not participate in the Kondo phenomenon. The phenomenon of reentrant superconductivity occurs in those materials for which the Kondo effect is also present. Hence, looking at X_d versus temperature for an individual orbit will determine whether or not the states on this orbit of the Fermi surface are in fact participants in the bulk Kondo phenomenon, and in reentrant superconductivity.

The dHvA effect will not see a Kondo-like (AF) minimum in X_d because the dHvA effect does not see the scattering effects of phonons on electrons at the Fermi surface.[28] Within the temperature range for which the dHvA effect is visible, we expected a $\ln T$-type behavior of the X_d for those orbits which are AF.[29] For those orbits which are not AF we expected X_d to be temperature independent.

The two orbits were chosen for observation in this portion of the study were (b) and (d) (see the Introduction for explanation of orbit labeling). Of the four orbits observed in this study, only (b) and (d) were of sufficient signal strength (due to their lower effective masses, shown in Table II) to permit significant temperature variation versus amplitude measurements to be made, as the dHvA signal amplitude diminishes exponentially with rising temperature.

Measurements were made on the $x=0.5$ at. % Ce and $x=0.5$ at. % Gd crystals. The results of these measurements are shown in Fig. 5. Also included for comparison is a plot of bulk resistivity versus $\ln T$ for a 0.5 at. % Ce crystal.

We note the following observations.

(1) Scattering due to the Ce impurity at a given temperature, for both orbits (b) and (d), is roughly twice that for the case of the Gd impurity.

(2) The (d) orbit shows a strong dependence of X_d upon temperature for the 0.5 at. % Ce crystal.

(3) The 0.5 at. % Gd crystal also shows a temperature dependence of X_d for orbit (d), although not quite as strong as in the case of Ce doping. In light of the fact that there is no bulk Kondo resistivity minimum for this material, the observation of a temperature dependence of

TABLE II. Effective masses of each cited orbit

Orbit	Experimentally determined orbitally-averaged effective mass
(a)	2.17
(b)	1.52[a]
(c)	2.18
(d)	0.55[a]

[a]Previously published values from Ref. 4.

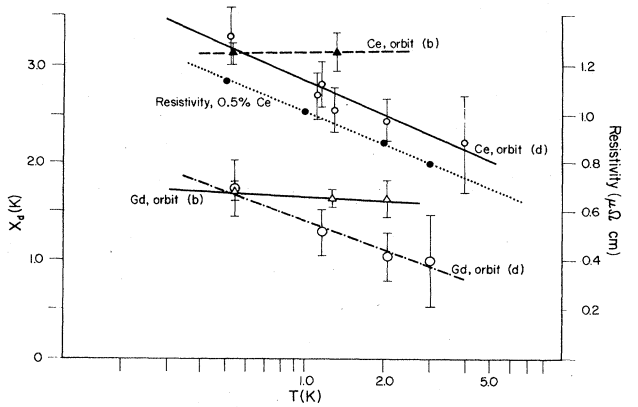

FIG. 5. Experimentally measured values of X_d versus $\ln T$ for $La_{1-x}Gd_xAl_2$ and $La_{1-x}Ce_xAl_2$, $x=0.5$ at. %, for orbit (b) and for orbit (d). Also plotted is bulk resistivity versus $\ln T$ for $La_{1-x}Ce_xAl_2$, $x=0.5$ at. % (from Ref. 13).

X_d in the Gd-doped crystal is a very surprising result.

(4) For orbit (d), there thus exists an AF temperature dependence of X_d for both Ce- and Gd-doped alloys.

(5) For orbit (b) no temperature dependence of X_d exists for either alloy.

From the above observations, the following conclusions are suggested. (1) The existence of Kondo phenomena is highly $\mathbf{k}$-dependent in $La_{1-x}R_xAl_2$. (2) It is possible for an alloy to show *no* bulk Kondo effects, i.e., $La_{1-x}Gd_xAl_2$, and yet have temperature-dependent (Kondo-like) impurity scattering on some orbits [i.e., orbit (d)] on the Fermi surface.

C. Dingle-temperature anisotropy

This portion of the study was done using the 0.3 at. % Ce crystal and the 0.5 at. % Gd crystal for orbits (a), (b), and (c) on the Γ-centered sheet. The 0.5 at. % Ce crystal showed too much scattering to obtain reliable X_d measurements for orbits (a) and (c).

The quantity X_d can be calculated as

$$X_d = K_0 m^* (\Delta \ln M / \Delta H) , \tag{6}$$

i.e., the slope of the graph of $\ln M$ versus $K_0 m^*/H$, where M is the amplitude of the dHvA signal. The value of X_d obtained from such a graph is a measure of the scattering of conduction electrons due to the presence of the magnetic impurity, provided the following conditions are met.

(a) One is far from the region of a SSZ (SSM). A SSZ will cause a minimum in the amplitude of the dHvA signal as the magnetic field is varied, in a manner exactly analogous to the behavior of a SSZ in a rotation diagram. In a rotation diagram the magnetic field is kept constant, and the product m^*g' is allowed to vary by varying the angle of the sample within the magnetic field. In this case of X_d measurements, m^* is constant but H varies, so $g'=g_0+H_{ex}/\mu_B H$ varies. The product m^*g' will vary, resulting in a SSZ occurring at that value of H such that $m^*g'=1,3,\ldots$.[30] In order to ensure that one is far from the region of a SSZ (or SSM), one must first be able to determine both m^*, and the effective g factor, g'.

(b) No spin-dependent scattering (SDS) exists. A difference of X_d for spin-up and spin-down electrons will cause the plot of $\ln M$ versus $K_0 m^*/H$ to deviate from straight-line behavior, as the contributions add vectorially, with their relative phase being dependent upon the magnitude of H.[6] A SSM seen in a plot of $\ln M$ versus $1/H$ will indicate the presence of SDS in the same manner as is evident in a SSM seen in a rotation diagram, i.e., the sharpness of the minimum is indicative of the amount of spin-dependent scattering. A calculated example is shown Fig. 6.

The procedure (known as dHvA wave-shape analysis) for determining g' and δx depends upon the measurement of the amplitudes and relative phases of the higher dHvA harmonics (see Ref. 6 for a detailed discussion of wave-shape analysis). Unfortunately, for the orbits studied in this work, effective masses were too great to permit observation of adequate higher dHvA harmonic amplitudes within the range of magnetic field and temperature available with the apparatus employed. In order to extract the maximum amount of information from the data recorded in this portion of the study, interpretation will be given in the light of observations from Sec. II A.

Figure 7 shows a plot of dHvA amplitude versus $1/H$ for the 0.3% Ce-doped crystal. The X_d plot for orbit (b) deviates somewhat from a straight line. The least-squares-fitted straight line gives a value of $X_d = 3.89$ K/at. % Ce. The fact that the plot is not quite linear, points to the possibility that a SSM lies just outside the observed magnetic field range. The X_d plot for orbit (c) shows a substantially greater slope: $X_d = 5.56$ K/at. % Ce. The data points to not fall on a straight line. An arrow in the figure indicates a possible SSM. If this is the case, the minimum is extremely shallow, indicative of strong SDS.

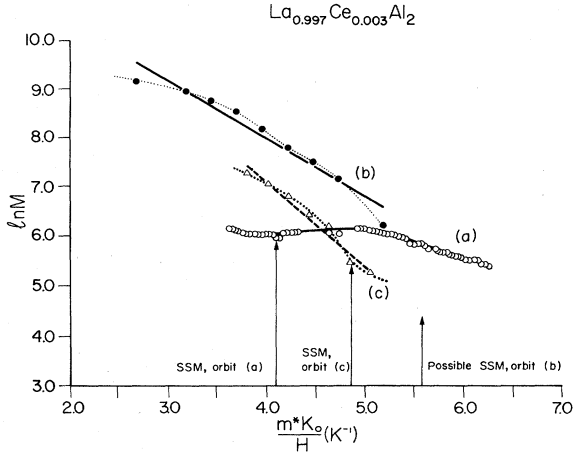

FIG. 7. Experimentally measured values of $\ln M$ versus m^*K_0/H on orbits (a), (b), and (c), for $La_{1-x}Ce_xAl_2$, $x = 0.3$ at. %, at $T = 0.55$ K. Arrows indicate positions of SSM's. Data for orbits (b) and (c) are shown with both a least-squares straight-line fit and an approximate curve fit. Error in amplitude measurement is represented by size of the data points, i.e., $\Delta M/M = 0.05$.

The X_d plot for orbit (a) has a very small slope. The slope at the low-field (50—54 kG) end of the curve is $X_d = 1.89$ K/at. % Ce. The prominent feature of this plot is the existence of a SSM. This feature is seen more clearly in Fig. 8. This data was obtained in the same manner as was that in Fig. 7; however, in Fig. 8 magnetic field values were chosen which are more uniformly spaced in $1/H$. An estimate of the amount of SDS can be calculated from

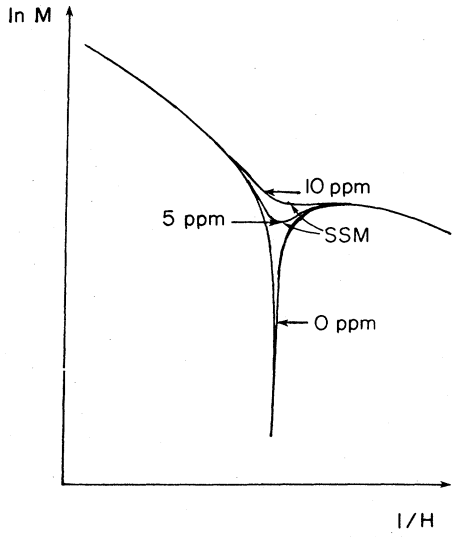

FIG. 6. Calculated spin-split minima (SSM) as a function of the amount of impurity within strong spin-dependent scattering. This example is due to R. Hendel (Ref. 31), and is appropriate for iron impurities in Cu-Cr alloys.

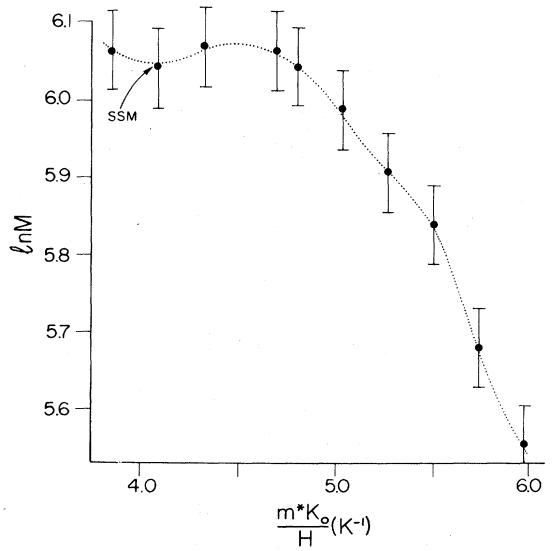

FIG. 8. $\ln M$ versus $K_0 m^*/H$ for $La_{1-x}Ce_xAl_2$, $x = 0.3$ at. %, for orbit (a). Arrow indicates position of SSM. Error bars represent $\Delta M/M = 0.05$.

$$P/Q=\exp(K_0 m^* \delta x/H)\,, \tag{7}$$

where P and Q are the amplitudes of the spin-up and spin-down contributions to the signal.[18] Using estimates for P and Q extracted from Fig. 8, $\delta x \cong 1.0$ K, or normalized to 1 at. % Ce, $\delta x \cong 3.3$ K/at. % Ce. It appears that the SDS is *extreme* for this orbit.

The values of δx calculated from the rotation diagrams, listed in Table I, when viewed with the above result of SDS at orbit (a), demonstrate that Ce causes spin-dependent scattering for dHvA orbits on the Γ-centered sheet of $LaAl_2$, with δx increasing as one goes [in the (110) plane] from [111] to [100]. That is, the coupling of the Ce impurity to the conduction electrons is seen to increase with increased conduction-electron f-wave character.

For the 0.5% Gd-doped crystal, amplitude versus $1/H$ is shown in Fig. 9. The X_d plot for orbit (b) is a straight line with $X_d=3.32$ K/at. % Gd. That there is virtually no SDS for this orbit can be inferred from the negligible amount of SDS present for the SSM (which is virtually a SSZ) located at [111]+5.6° (see Table I).

The X_d plot for orbit (c) has a very high slope, $X_d=8.10$ K/at. % Gd. This large slope can be caused by (1) a large amount of scattering of conduction electrons from their orbits, and/or (2) a SSM which occurs at a magnetic field value just below the range of observation of the dHvA signal. If (1) is true, then a comparison of X_d for this orbit and the orbit (b), together with the partial-wave character for each orbit, will illuminate which partial-wave component(s) of the host wave function is a strong participant in the interaction. If (2) is true, then firm conclusions can be reached only when data at lower temperatures, which will permit observation at lower magnetic fields, become available.

The plot of $\ln M$ versus m^*K_0/H for orbit (a) has a slope of $X_d=3.32$ K/at. % Gd at ~50 kG, and $X_d=0.72$ K at ~80 kG. The low-field value of X_d is comparable to the X_d of orbit (b). It appears that the field range for this plot is just below the magnetic field value needed for a SSM to be observable. Verification of this hypothesis requires apparatus capable of higher magnetic field values.

The hypothesized SSM which may be responsible for the steepness of slope of the X_d plot for orbit (c), and also for the curvature of the X_d plot for orbit (a) in the Gd-doped crystal, is consistent with the appearance of a SSM in the rotation diagram of the Gd-doped crystal at [111]−31°. This can be seen as follows: An interpolation of effective mass gives a value of $m^* \sim 2.14$ for the [111]−31° orbit; this mass is very close to the measured mass for orbits (c) and (a). Hence it is quite plausible that a SSM could be just out of magnetic field range on the X_d plots of both of these orbits.

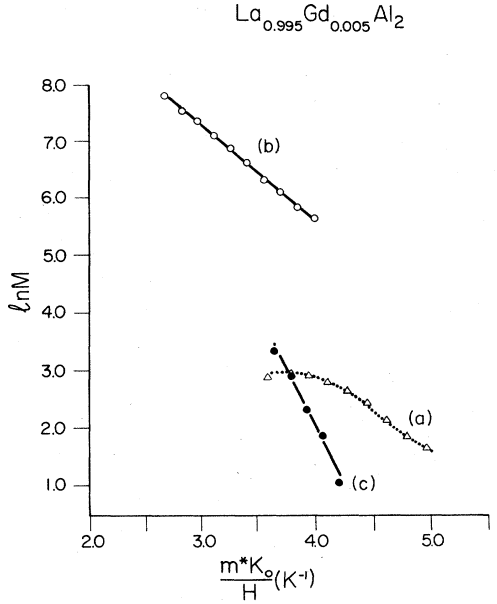

FIG. 9. Experimentally measured values of $\ln M$ versus m^*K_0/H, for $La_{1-x}Gd_xAl_2$, $x=0.5$ at. %, at $T=0.55$ K, orbits (a), (b), and (c). Error bars for data points on each of the curves represented by the size of the data points, i.e., $\Delta M/M=0.05$.

III. SUGGESTIONS FOR FUTURE STUDY

In order to more systematically and quantitatively describe the interactions between the magnetic impurity Ce (or Gd) and conduction electrons of $LaAl_2$, a calculation of the APW partial-wave coefficients $(\partial A/\partial \eta_l)$ (Ref. 32), for several different orbits on several sheets of the Fermi surface of the host matrix needs to be carried out.

Further insights into the behavior of $LaAl_2$ doped with Ce or Gd can be gained experimentally by making dHvA measurements at higher magnetic fields and lower temperatures. It is hoped that the confirmation of scattering anisotropy on the Fermi surface of $LaAl_2$ demonstrated in this work will stimulate theorists to reexamine the MH-Z theory of reentrant superconductivity, and begin incorporating features of band structure into its assumptions.

ACKNOWLEDGMENTS

This work was supported by National Science Foundation Grant No. DMR 78-06271. The authors wish to thank R. DeGroot, Katholieke Universiteit Nijmegen, for communicating his preliminary, unpublished band-structure results, A. Hasegawa for communicating his unpublished effective-mass calculations for the Γ-centered sheet of Fermi surface, and B. Lengeler for providing the $La_{0.995}Gd_{0.005}Al_2$ sample.

*Present address: Solid State Division, Oak Ridge National Laboratory, Oak Ridge, TN 37830.

[1]E. Muller-Hartmann and J. Zittartz, Phys. Rev. Lett. **26**, 428 (1971).

[2]A. Hasegawa and A. Yanase, J. Phys. F **10**, 847 (1980).

[3]A. C. Switendick, in *Proceedings of the 10th Rare Earth Research Conference* (Carefree, Arizona, 1973), edited by C. J. Kevane and T. Moeller, National Technical Information

Service Note 730402 P1 (U.S. Atomic Energy Commission, Oak Ridge, Tennessee, 1973), Vol. 1, p. 235.
[4]E. Seitz, B. Lengeler, G. Kamm, and J. Kopp, J. Phys. (Paris) Colloq. **40**, C5-76 (1979).
[5]J. Reichelt and K. Winzer, Phys. Status Solidi B **89**, 489 (1978).
[6]R. J. Higgins and D. H. Lowndes, *Electrons at the Fermi Surface,* edited by M. Springford (Cambridge University Press, Cambridge, 1980), Chap. 10.
[7]Y. Chung, D. H. Lowndes, and C. Lin-Hendel, J. Low Temp. Phys. **32**, 599 (1978).
[8]M. B. Maple and T. F. Smith, Solid State Commun. **7**, 515 (1969).
[9]A. A. Abrikosov and L. P. Gor'kov, Zh. Eksp. Teor. Phys. **39**, 178 (1960) [Sov. Phys.—JETP **12**, 1243 (1961)].
[10]A. C. Switendick (private communication) has also suggested that the smaller holelike sheets of Fermi surface have a high degree of f-wave character, possibly as much as 34%.
[11]R. deGroot, F. M. Mueller, and D. D. Koelling, unpublished results (private communication).
[12]D. Davidov, A. Chelkowski, C. Rettori, R. Orbach, and M. B. Maple, Phys. Rev. B **7**, 1029 (1973). Also, B. R. Coles, D. Griffith, R. J. Lowin, and RT. H. Taylor, J. Phys. C **3**, L121 (1970).
[13]F. Steglich, Z. Phys. B **23**, 331 (1976).
[14]M. B. Maple, Ph.D. dissertation, University of California, San Diego, 1969.
[15]M. Beyss, J. M. Welter, and T. Kaiser, J. Cryst. Growth **50**, 419 (1980).
[16]M. B. Maple, W. A. Fertig, A. C. Mota, L. E. DeLong, W. Wohlleben, and R. Fitzgerald, Solid State Commun. **11**, 829 (1972).
[17]G. Riblet and K. Winzer, Solid State Commun. **9**, 1663 (1971).
[18]P. T. Coleridge, G. B. Scott, and I. M. Templeton, Can. J. Phys. **50**, 1999 (1972).
[19]Y. K. Chang and R. J. Higgins, Phys. Rev. B **12**, 4276 (1975).
[20]A. Hasegawa, unpublished results (private communication).
[21]B. Lengeler, in *Electronic Structure of Noble Metals,* Vol. 82 of *Springer Tracts in Modern Physics,* edited by G. Höhler (Springer, New York, 1978), pp. 14—17.
[22]D. L. Randles, Proc. R. Soc. London, Ser. A **331**, 85 (1972).
[23]A. M. Clogston and P. W. Anderson, Bull. Am. Phys. Soc. **6**, 124, FA7 (1961).
[24]J. Kondo, Prog. Theor. Phys. (Kyoto) **28**, 846 (1962).
[25]P. G. deGennes, J. Phys. (Paris) **23**, 630 (1962).
[26]R. E. Watson, S. Koide, M. Peter, and A. J. Freeman, Phys. Rev. **139**, A167 (1965).
[27]R. E. Watson, A. J. Freeman, and S. Koide, Phys. Rev. **186**, 625 (1969).
[28]S. Englesberg and G. Simpson, Phys. Rev. B **2**, 1657 (1970).
[29]J. Kondo, Progr. Theor. Phys. (Kyoto) **32**, 37 (1964).
[30]P. T. Coleridge and I. M. Templeton, Phys. Rev. Lett. **24**, 108 (1970).
[31]R. R. Hendel, Ph.D. dissertation, University of Oregon, 1979.
[32]See, for instance, P. T. Coleridge, N. A. W. Holswarth, and M. G. Lee, Phys. Rev. B **10**, 1213 (1974).